

# Beyond Correlation: A Path-Invariant Measure for Seismogram Similarity

Joshua Dickey, Brett Borghetti, William Junek, and Richard Martin

April 2019

## ABSTRACT

Similarity search is a popular technique for seismic signal processing, with template matching, matched filters and subspace detectors being utilized for a wide variety of tasks, including both signal detection and source discrimination. Traditionally, these techniques rely on the cross-correlation function as the basis for measuring similarity. Unfortunately, seismogram correlation is dominated by path effects, essentially requiring a distinct waveform template along each path to be detected. To address this limitation, we define a path-invariant measure for seismogram similarity. A deep convolutional neural network with a triplet loss function maps raw seismograms to a low dimensional embedding space, where nearness on the space corresponds to nearness of source function, regardless of path or recording instrumentation. This path-agnostic embedding space represents a new representation for seismograms, characterized by robust, source-specific features. The dataset used to train and test the algorithm comes primarily from the USArray experiment, a temporary network of 400 seismometers that was deployed at more than 2000 locations across the US from 2007 to 2012. The first four years (2006, 2007, 2008, 2009) were selected as the training set, and the following two years (2010, 2011) were selected for validation and testing. The training, validation and test sets contained 24,811, 5,711 and 4,214 seismograms, respectively. The utility of our novel embedding space representation is evaluated across three common seismic tasks: event association, signal detection, and source discrimination, achieving an accuracy

of 80%, 92% and 90%, respectively, all while minimizing the number of template waveforms required.

## INTRODUCTION

Seismograms are time-series records of the earth’s motion at a fixed station. This motion results from seismic waves, that have often traveled a considerable distance from the source event, and seismograms reflect the combined influence of both the source itself, and the propagation path between source location and recording station (Bormann and IASPEI, 2012). As illustrated in Fig. 1, two seismograms depicting different events yet sharing a common path can appear similar. This fact has long been recognized by the seismic community (Stauder and Ryall, 1967; Kanamori and Ishida, 1978). In the earliest days of manual processing and helicorders, analysts were often able to identify mining events from a particular mine, recorded at a particular station, by simply comparing the visual similarity of new seismograms to previously recorded examples (Israelsson, 1990). In fact, a common practice was to take two translucent paper seismograms and compare them, by passing the waveforms across one another while holding them up to a light source (Schulte-Theis and Joswig, 1993). Thus began the science of seismogram similarity. Of course, the advent of computer processing ushered in the development of a multitude of techniques to exploit these similarities algorithmically. Case-based discrimination (Dysart and Pulli, 1987), template matching (Giannakis and Tsatsanis, 1990), waveform correlation (Harris, 1991), subspace detection (Harris, 2006) and similarity search (Yoon et al., 2015) are all similarity-based algorithms which have been proposed over the last several decades, and deployed against a wide range of seismic signal processing tasks, such as discriminating mining blasts, screening swarm events, identifying aftershock sequences, and even detecting general seismic signals.

While these algorithms have different tasks ranging from discrimination to detection, fundamentally they are all examples of similarity-based classifiers (Chen et al., 2009), which estimate the class label of a new seismogram based on its similarity to one or more previously labeled templates. Furthermore, these similarity-based classifiers all share a common measure of similarity: cross-correlation. Such methods are generally referred to as correlation

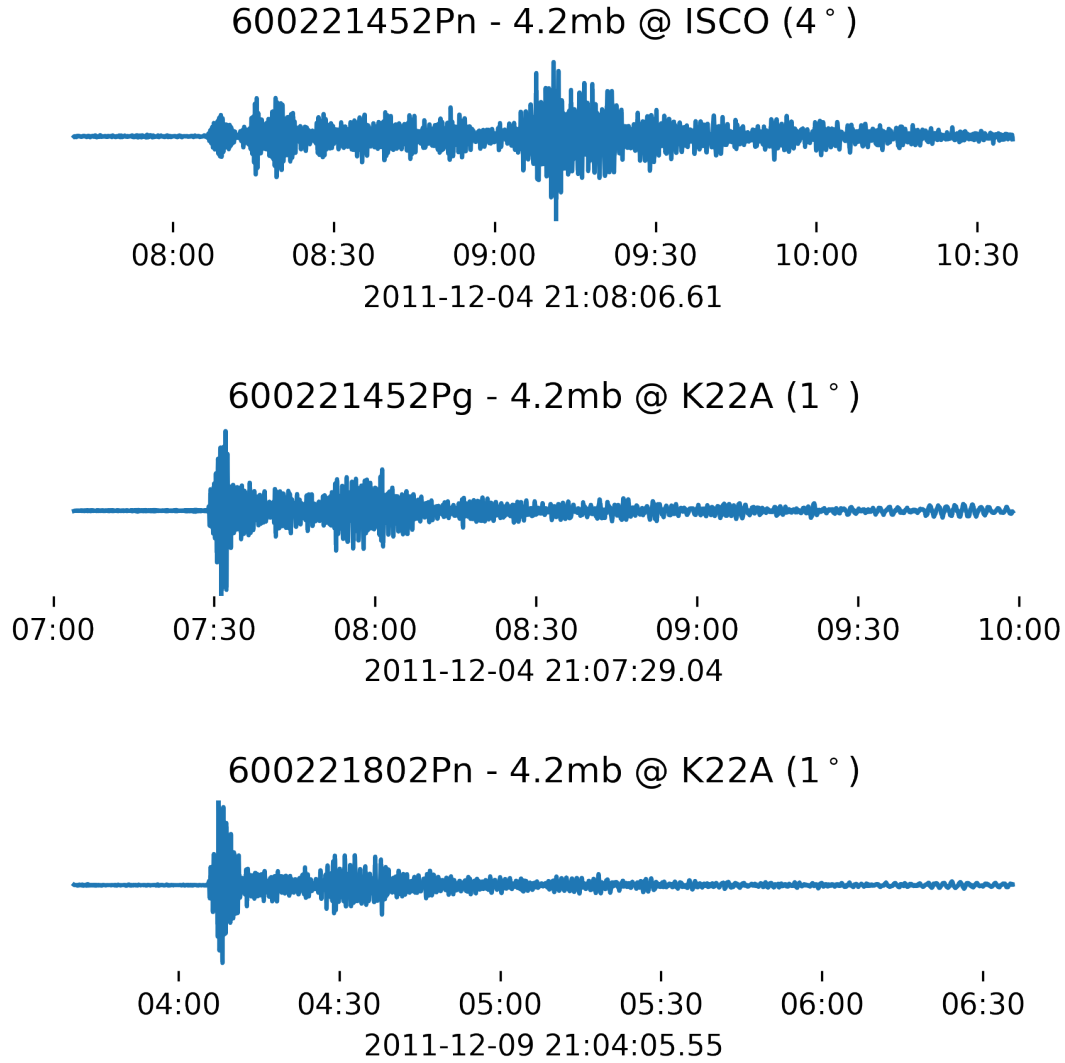


Figure 1: Three Seismograms depicting explosions at a coal mine near Thunder Basin, WY. The first two seismograms depict a common source event (600221452), recorded at two separate seismic stations, ISCO and K22A respectively. The third seismogram depicts a nearby event (600221802), also recorded at K22A. The first and second waveforms depict the same event recorded at different stations, while the second and third waveforms depict different events which share a common path. The correlation between the first and second source-similar waveforms is only 0.03, and the waveforms visually appear quite different. On the other hand, the visual similarity between the second and third path-similar seismograms is obvious, and they are correlated with a coefficient of 0.18. This illustrates the path-dominant similarity associated with seismogram correlation.

detectors (Harris, 2006).

This common reliance on correlation is concerning, because the correlation coefficient of two seismograms is dominated by path effects (Schulte-Theis and Joswig, 1993), as demonstrated in Fig. 1. While path-dominant similarity can be desirable, such as when detecting aftershock sequences from a particular fault, or mining blasts from within a small quarry, in general, path-dominant similarity is problematic, as source-similar signals de-correlate with even slight deviations in path (Harris, 2006). This includes deviations in origin location, such as two explosions occurring at different points in a mining quarry, and deviations recording location, such as two recordings of the same explosion by separate seismic stations in a regional seismic array. In either case, path differences of even just a quarter wavelength can significantly degrade the correlation of two seismograms (C. Pechmann and Kanamori, 1982; Motoya and Abe, 1985). As such, the vast majority of events (82%) are undetectable using correlation detectors (Dodge and Walter, 2015).

This work presents a new measure for seismogram similarity that bypasses correlation entirely, and that is designed to be both path-invariant and source-specific. To be precise, the design goal is to create a measure of seismogram similarity that enables the identification of seismograms sharing a common source event, regardless of the path of travel. While such a measure was previously computationally intractable, it is possible with the careful application of deep convolutional neural networks (CNNs). In 2019, researchers at the Los Alamos National Laboratory published a method using a CNN to predict the pairwise association of seismic phase arrivals, for 6 second windows, across a local group of 6 stations in northern Chile, reporting an accuracy of over 80% (Delorey et al., 2019). Building on these results, we construct a source-dominant, path-invariant measure for seismogram similarity which operates on 180 second windows and is generalized across more than 1,000 sensors across North America. We do this by utilizing a state-of-the-art machine learning technique from the field of facial recognition, called a Triplet Network, which not only indicates pairwise association between seismograms, but actually maps the seismograms to low-dimensional vectors, called embeddings, such that the embedding space distance between seismograms sharing a common source event are minimized, regardless of path, while remaining distinct from any other events. This embedding strategy is displayed in Fig. 2. In this way, the

embedding function becomes a rich feature extraction technique for source-specific and path-invariant features.

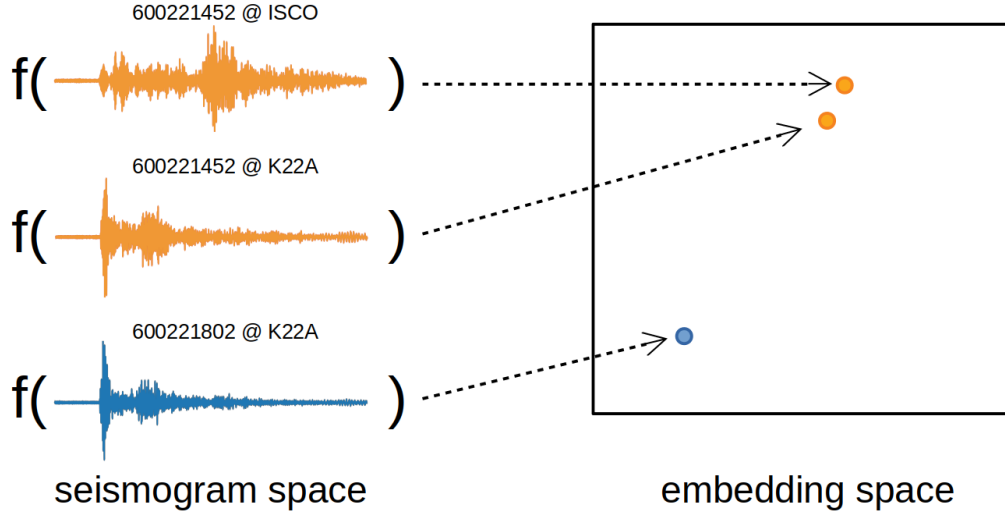


Figure 2: Path-Invariant Embedding Function for Seismograms. The embedding function,  $f(\cdot)$ , is a non-linear transformation that maps time-series seismograms to low-dimensional embeddings. The mappings should be path-invariant and source-specific, such that regardless of the recording station, all seismograms associated with a particular event are mapped closely in the embedding space, and seismograms not associated with that event have more distant embeddings. This embedding function can be learned using a convolutional neural network architecture, trained with seismogram triplets.

The triplet network architecture accepts three observations - two similar and one different from the others. Training a triplet network to learn seismic source similarity requires source-similar seismogram triples: two of the three waveforms are associated with a common source event and the third waveform is not. For this task, it is preferable to have a training set containing seismograms recorded from a densely-spaced sensor network, so that the neural network can experience seismograms recordings across numerous paths for the same event. The the 400 three-channel broadband sensors of the USArray experiment provided an ideal dataset of seismograms; data from this array is used for training and testing. The triplet network is trained against 4 years of data (2006, 2007, 2008 and 2009), validated against a single year of data (2010), and tested against a final year of data (2011).

The value of this path-invariant measure is demonstrated through performance evaluation on three common seismic tasks: event association, signal detection and source discrimination. The event association task of determining whether or not two waveforms depict the same event achieves a binary accuracy of 80%. This accuracy is achieved using only the waveform characteristics, without information on times or recording locations, and the technique has strong potential to augment existing methods of event association (Delorey et al., 2019).

The signal detection task achieves similar performance to correlation detectors when using a broad catalog of templates taken from the station under test (using the area under the receiver operating characteristic curve, or AUC, as a metric, our performance is 91.7% vs 91.8% for the correlation detector). However, when applying these same templates to a novel station, our path-invariant measure outperforms traditional correlation, achieving an AUC of 87% compared to 65% for the traditional detector.

The real promise of the technique, however is for source discrimination. The embedding space is a rich basis for source-specific seismic feature extraction (Hadsell et al., 2006). An explosion discriminator achieves 90% accuracy with no explicit training for the source discrimination task; the discriminator simply compares the similarity of unknown waveforms to a randomly-selected set of 10 explosion templates. This technique is often referred to as one-shot learning (Koch et al., 2015), and shows promise for discrimination of novel sources when only a few extant templates are available.

In the remainder of this work, these contributions and conclusions are explored in detail, by reviewing the related literature, outlining methodology, and detailing and discussing our results.

## BACKGROUND

This work merges two relatively disparate fields of science. On the one hand, the application is seismogram similarity, a field with a rich history and considerable previous research. On the other hand, the methodology employs learned similarity, a relatively nascent field that has principally been associated with machine learning image processing applications. This background section is divided into three distinct subsections: seismogram similarity; learned

similarity; and learned seismogram similarity. Each subsection contains a brief background and literature review, as well as a discussion of the limitations and gaps in the current research, which our work attempts to fill.

## Seismogram Similarity

To lay the foundation for a discussion of seismogram similarity, it is first important to discuss the nature of the seismogram. Seismometers are stationary instruments, which produce sensitive time-series measurements of either the velocity or acceleration of the ground at a fixed location on the earth. Because the seismometer is stationary, and because the epicenter of most seismic events is inherently variable, most seismic recordings (commonly referred to as seismograms) are recorded at some distance from the epicenter of the event. Due to this distance, the seismogram always represents the composition of several effects, including the seismic source itself, the propagation path from the source to the seismometer, the frequency response of the seismometer, as well as any ambient noise at the seismometer’s location (Bormann and IASPEI, 2012). Each of these components is useful in its own right: The source effects contain information about the energy release (magnitude and moment), source type (explosion, earthquake, volcano, etc) and faulting geometry (focal mechanism); the path effects encode the structure of the earth (crust, core, mantle), subduction zones, as well as the physical states of different layers; the instrument response describes the internal characteristics of the seismometer; and finally, the ambient noise is affected by anthropogenic encroachment. Because of this diverse composition inherent to each seismogram, estimating seismogram similarity can be quite challenging, and each similarity-estimating technique may be affected differently by the underlying components. It is therefore important to understand the different methods for similarity estimation, and how each type of similarity estimator works.

The traditional measure for seismogram similarity is the cross-correlation function. This measure has been used for detecting and discriminating seismic signals since the late 1980s (Dysart and Pulli, 1987), and such techniques are commonly referred to as correlation detectors (Harris, 2006). Correlation detectors are exquisitely sensitive, allowing detections near the noise floor for known repeating events in highly confined geographical regions (Gibbons and Ring-

dal, 2006). Unfortunately, this confinement is also a limitation, as seismogram correlation has been shown to decay exponentially with even minor differences in path distance (Israels-son, 1990). In fact, early research suggested that correlation-based similarity was limited to signals with hypo-centres separated by no more than a quarter wavelength (Frankel, 1982; Motoya and Abe, 1985), although later efforts have since shown improvements, allowing the correlation length to be up to two wavelengths (Harris, 1991). Additionally, researchers have also shown that seismograms quickly decorrelate across small variations in mechanism and source function (Hutchings and Wu, 1990). These facts limit the applicability of the correlation detector to only the most repetitive sources that are confined to localized geographical regions (Harris, 2006). To relax these constraints, there have been numerous adaptations proposed.

To address variations in ambient noise, narrow bandpass filters were applied (Israels-son, 1990). To address minor variations in mechanism, composite templates were employed, derived from linear combinations of several master templates representing a range of mechanisms (Harris, 1991). To address path effects, dynamic waveform matching was developed, introducing a non-linearity to the correlation, allowing relative stretching or squeezing of the template (Schulte-Theis and Joswig, 1993). Subspace detectors attempt to address all of these variations at once, with even more robust composite templates (Harris, 2006). Recently, efforts focused on a multiplicity of templates and a computationally efficient search across them (Yoon et al., 2015; Zhang and Wen, 2015; Beaucé et al., 2017; Bergen and Beroza, 2018b). Despite all these efforts to date, even the most advanced correlation detectors are not generally applicable to seismic detection, as only 18% of all global events possess sufficient similarity to be detected by these methods (Dodge and Walter, 2015).

In summary, cross-correlation is fundamentally limited as a measure of seismogram similarity, due to its inherent path-dependence. We assert that a better measure is needed, and that the ideal measure of seismogram similarity should be invariant to path, instrumentation and ambient noise. In other words, the measure should be based entirely upon the similarity of the originating source functions. Such a measure could enable general detection from a relatively small set of template waveforms. Additionally, it could be an ideal means of performing template-based source discrimination, as nearness in similarity would unambigu-



ously imply nearness of source. One way to search for functions is through machine learning - the next section explores machine learning-based similarity techniques from other domains which could be applied in the seismic domain.

## Learned Similarity

Each of the traditional seismogram similarity measures discussed so far has been fundamentally built around the cross-correlation function. However, it is interesting to note that almost none of the measures performed cross-correlation directly on the raw waveforms. Instead, each of these measures first applied some pre-processing function to the raw waveforms, either linear (time shifts, bandpass filters, linear combinations) or non-linear (dynamic time warping) prior to performing cross-correlation. We can generally understand these pre-processing functions to be mappings, from raw waveform space to a new *embedding space*. In each case, the mapping function is chosen such that the cross-correlation of two objects in the embedding space meets some desired similarity objective.

As it turns out, this embedding process used in traditional correlation-based similarity closely mirrors the process accomplished in machine learning-based similarity. For learned similarity, a parameterized embedding function architecture is established, and the parameters are optimized such that the distance between two objects in the space achieves the desired similarity objective. Over the last several years, such learned similarity measures have revolutionized the field of facial recognition in particular and the field of image processing in general, fueling advances in image recognition (Wang et al., 2014), object tracking (Leal-Taixe et al., 2016) and even vision navigation (Kumar et al., 2016). In the remainder of this section, we review some of the state of the art techniques available for constructing deep learned similarity measures, focusing particularly on the embedding function architecture and similarity objective, in turn.

### *Embedding Function Architecture*

Many early efforts to create learned similarity spaces utilized a linear architecture, such as the Mahalanobis distance (Xing et al., 2002; Jain et al., 2008, 2009). However, in recent years,

much success has been gained by employing non-linear architectures (Belkin and Niyogi, 2003), particularly in the form of deep convolutional neural networks or CNNs (Hadsell et al., 2006). These CNNs were originally developed with 2-dimensional kernels, or filters, which allowed them to closely model the hand-crafted kernels traditionally used in image processing (LeCun et al., 1989). To adapt these powerful CNN architectures to process time-series waveforms, 1-dimensional CNNs were developed (Burges et al., 2003), enabling learned similarity spaces for audio waveforms (Jang and Yoo, 2009).

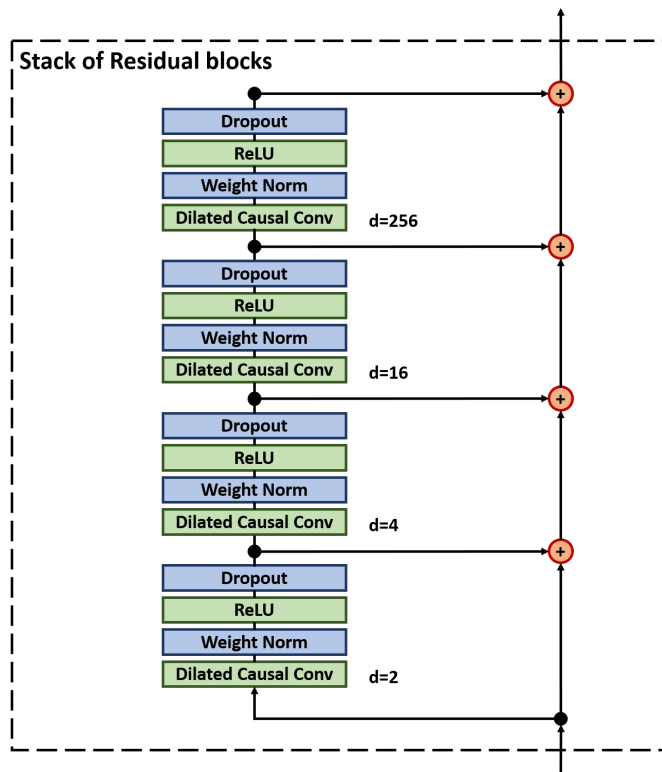


Figure 3: A single stack of 4 dilated residual blocks commonly found in a Deep Temporal Convolutional Neural Network Architecture. In this case, the residual blocks have exponentially increasing dilation rates, increasing from 2 to 256 across the 4 blocks. This rapid dilation provides the network a wide receptive field which is critical for learning long-period features frequently found in time-series waveform data.

A more recent advancement to the traditional CNN architecture is the Temporal Convolutional Network (TCN), which is characterized by layered stacks of dilated causal convolutions and residual connections (Bai et al., 2018), as illustrated in Fig. 3. Such an architecture is

particularly applicable to time-series waveforms with long-period dependencies, and offers several distinct advantages for seismic feature extraction (Dickey et al., 2019), including:

- Residual connections allow the model to have high-capacity and stable training.
- Dilated convolutions allow precise control over the receptive field.

The receptive field is of primary importance for time-series modeling, as it explicitly limits the learnable feature periodicity at a given layer. The equation for calculating the receptive field,  $r$ , for a given convolutional layer,  $l$ , kernel size  $k$ , and dilation rate,  $d$  is given in (1):

$$\begin{aligned} r_l &= r_{l-1} + d(k - 1) \\ \text{where } r_0 &= 0 \end{aligned} \tag{1}$$

In summary, the TCN is ideally suited for the efficient embedding of seismograms. This architecture presents a rich search space for learning an optimal embedding function. However, optimizing this function requires defining a suitable similarity objective, detailed next.

### ***Similarity Objective***

Defining a quantitative similarity objective begins with a qualitative understanding of what similarity means for the given task, which is often referred to as a semantic definition of similarity. Once the semantic definition is established, the next step is to approximate it with an embedding function, such that nearness in the embedding space implies the semantic similarity (Chopra et al., 2005). This embedding function is learned via back-propagation of loss,  $\mathcal{J}$ , that reinforces the semantic definition.

One of the simplest semantic definitions of similarity is the concept of a *match*, where a matched pair of objects share a common identity, and an unmatched pair objects have different identities. For example, in the facial recognition task, a matched pair is defined as two images of the same person and an unmatched pair is defined as two images of distinct persons. The similarity objective is to optimize the parameters of the embedding function such that the embedding space distance between matched pairs is small, while the distance between unmatched pairs is large. This embedding function can be learned directly by a

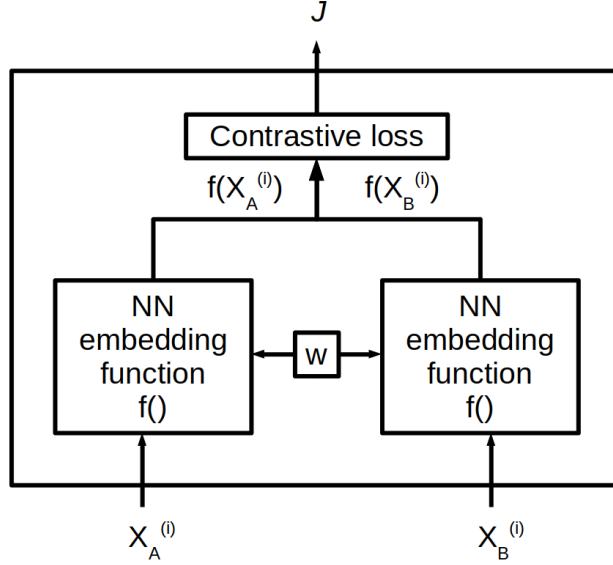


Figure 4: Siamese Neural Network.

Siamese Neural Network, which takes in a batch of  $m$  object pairs, of which half are matched, and half are unmatched. The two objects,  $X_A^{(i)}$  and  $X_B^{(i)}$ , are then embedded via twin copies of the embedding function,  $f(\cdot)$ , with tied parameter weights  $w$ , as shown in Fig. 4. The parameters of the embedding function are updated via the contrastive loss function, which penalizes two contrasting cases: matched pairs are penalized for being embedded too far apart and non-matched pairs are penalized for being embedded too close together with respect to some margin,  $\alpha$ , as given in Eq. (2) and Eq. (3), respectively (Chopra et al., 2005).

$$\mathcal{J} = \sum_{i=1}^{m/2} \left[ \left\langle f(X_A^{(i)}), f(X_B^{(i)}) \right\rangle \right] \quad (2)$$

$$\mathcal{J} = \sum_{i=1}^{m/2} \left[ \alpha - \left\langle f(X_A^{(i)}), f(X_B^{(i)}) \right\rangle \right]_+ \quad (3)$$

where  $[\ ]_+$  indicates the ramp function.

This technique works well, however, one drawback is the relatively inefficient use of the embedding space. Matches are too greedy, as the Siamese Network attempts to map all matches to a single point in the space. Meanwhile, non-matches are inefficient, pushed apart only a fixed distance (Hoffer and Ailon, 2015). As a result, the Siamese Network is used less

frequently in favor of the Triplet Network, which we shall next discuss.

The Triplet Network is similar to the Siamese Network (Hoffer and Ailon, 2015), however it is trained on batches of  $m$  triples, where each triple is comprised of an anchor object,  $X_A^{(i)}$ , a positive object,  $X_P^{(i)}$ , and a negative object,  $X_N^{(i)}$ . From within each triple, both a matched and non-matched pair can be constructed, however, the triplet loss function computes the relative embedding distance between the matched pair and non-matched pair, and no loss is accrued as long as the matched pair is closer by some margin,  $\alpha$ , as given in Eq. (4).

$$\mathcal{J} = \sum_{i=1}^m \left[ \left\langle f(X_A^{(i)}), f(X_P^{(i)}) \right\rangle - \left\langle f(X_A^{(i)}), f(X_N^{(i)}) \right\rangle + \alpha \right]_+ \quad (4)$$

where  $[ ]_+$  indicates the ramp function.

The Triplet network avoids the greediness of the Siamese network, and makes more efficient use of the embedding space, however it has its own drawbacks. Particularly, it can converge quickly at first, but learning slows rapidly, as the majority of the negative pairs are pushed beyond the margin, failing to train the weights appreciably. This can be solved by sampling hard pairs, semi-hard pairs and several other sampling strategies, all of which rely on iterative processing via forward propagation to determine embedding space distances, selectively sampling based on those distances, and then applying back propagation on the sample (Hermans et al., 2017). The algorithm used to sample hard pairs is commonly referred to as the *batch hard* loss function, and it requires that each batch be composed by randomly sampling  $L$  distinct identities and then randomly sampling  $K$  examples of each identity. In this way, the total number of objects in a batch is  $L * K$ , and each object is double indexed so that object  $X_u^{(v)}$  represents the  $u_{th}$  example of the  $v_{th}$  identity. The triplet loss is calculated using Eq. (4), except that in this case, every object in the batch is treated as an anchor  $X_A^{(i)}$ , and used to form a new triplet by selecting the *hardest* positive and *hardest* negative samples,  $X_P^{(i)}$  and  $X_N^{(j)}$  respectively, for that anchor within that batch, as detailed in Eq. (5).

$$\mathcal{J} = \sum_{i=1}^{\overbrace{L}^{\text{all anchors}}} \sum_{A=1}^K \left[ \overbrace{\max_{\substack{P=1 \dots K \\ P \neq A}} \left\langle f(X_A^{(i)}), f(X_P^{(i)}) \right\rangle}^{\text{hardest positive}} - \overbrace{\min_{\substack{j=1 \dots L \\ N=1 \dots K \\ j \neq i}} \left\langle f(X_A^{(i)}), f(X_N^{(j)}) \right\rangle}^{\text{hardest negative}} + \alpha \right]_+ \quad (5)$$

where  $[ ]_+$  indicates the ramp function.

## Deep Seismogram Similarity

Deep Neural Networks are now being used across many areas of seismological research, from earthquake detection to earthquake early warning systems, ground-motion prediction, seismic tomography, and even earthquake geodesy (Kong et al., 2018). However, no effort has been made to date to use deep neural networks to build a seismogram similarity metric. The closest related work was in early 2019, where researchers at Los Alamos National Labs published a paper describing a convolutional neural network for the pairwise association of seismograms depicting a common event, regardless of path (Delorey et al., 2019). This work shows that path-invariant features do exist within the seismogram record. The seismograms considered in their work had a signal length of 6 seconds, and were restricted to recordings from 6 seismic stations. To process the signals, they used a shallow CNN with 4 layers, the input accepting two seismograms, the output producing a single boolean. In this way, their technique can be generalized as a simplified Siamese network, without tied weights. The lack of tied weights means there is no embedding layer, which prevents their technique from being used for feature extraction. And the small number of stations limits the generalizability and transportability of their algorithm. Finally, the short signal length (6 s) limits each individual seismogram to containing a single phase arrival, thereby limiting its ability to extract long-period features, such as P and S wave energy ratios, which are particularly pertinent to general source discrimination tasks.

## METHODOLOGY

We present a novel seismogram similarity measure, based on a learned embedding function, that is both source-dominant and path-invariant. We show that the resultant embedding space is a rich representation space for seismic signals, useful for performing similarity-based classification against three common class dichotomies for seismograms: common event vs different events (event association), signal vs noise (signal detection) and earthquake vs explosion (source discrimination). The remainder of this section describes the embedding function architecture, the similarity objective, the USArray dataset and the evaluation criteria for the three tasks.

## Embedding Function Architecture

The goal is to learn a path-invariant embedding function for seismograms, useful for source discrimination at up to regional distances. This is accomplished using a hybrid architecture with two distinct parts: First, a TCN is employed with a receptive field wide enough to capture both P and S wave phases; second, a densely connected output layer, with 64 nodes, is employed to facilitate a rich low-dimensional embedding space.

Using Eq. (1), the TCN is designed to have an overall receptive field of roughly 100 seconds (4000 samples), allowing it to learn long-period features down to 0.01 Hz, with just four dilated convolutional layers, as shown in Table 1. The TCN architecture consists of two residual stacks, shown in Fig. 3, each with 50 filters and a kernel size (filter length) of 16 samples. Finally, the TCN output is encoded by a densely connected output layer with 64 nodes, and the final output vector is normalized to have unit length. This results in 783,819 trainable parameters, and a network which reduces the three-channel 21,600 dimensional input into just 64 dimensions, for a 99.7% reduction in dimensionality.

Table 1: TCN Layer Parameters

<b>l</b>	<b>k</b>	<b>d</b>	<b>Receptive Field</b>
1	16	2	31
2	16	4	91
3	16	16	331
4	16	256	4171

## Similarity Objective

This embedding function is learned via a Triplet Network with batch-hard loss. Specifically, the batch size was set at 100, with  $L$  (the number of distinct source events in a batch) and  $K$  (the number of seismogram recordings for each event in a batch) both set equal to 10. In this way, each batch consists of 100 randomly selected seismograms, evenly represented across 10 different source events. These values were selected primarily on the basis of availability, since increasing  $K$  beyond 10 would have limited the dataset ( 95% of the events in the

USArray dataset were recorded by at least 10 stations), and increasing  $L$  beyond 10 would require more memory than the 12Gb available in the Nvidia 1080Ti GPU used for training.

Embedding space distances are computed using the  $L_2$  Norm. Because the output of the embedding function is normalized, the embedding space vectors are all constrained to a hypersphere with radius = 1. This ensures a bounded distance between any two embeddings, as chord lengths are always bounded by  $[0,2]$  for any unit hypershpere. Because these pairwise distances are bounded, a fixed margin can be used throughout training (Sidiropoulos, 2014). In this work, the margin is fixed at  $\alpha = 0.2$ , which is common (Schroff et al., 2015).

## Data Collection

Learning a path-invariant measure for seismogram similarity requires a training dataset with many recordings of a single seismic event across many disparate paths. This is best accomplished by a dense network of seismometers across a wide region. The USArray dataset is ideally suited for this endeavor.

The USArray Transportable Array consists of 400 temporary seismic instruments that were deployed at more than 2,000 temporary station locations across the Continental US between 2007 and 2015 (Busby et al., 2018). Each station utilized a broadband 3-channel (North-South, East-West and Vertical) instrument, installed in a post-hole configuration and digitized at 40 Hz. The instruments were generally one of three types, Guralp CMG3T, Quantera STS, or Nanometrics Trillium; the digitizers were primarily Kinometrics Q330, Q680 or RefTek. In this work, we have focused on the western portion of the array, with a dataset that includes 740 stations recording 1,105 distinct seismic events for a total of 34,736 seismograms. A map detailing the layout of the stations is shown in Fig. 5. For each of the 34,736 seismograms, a 180-second window is selected which includes the 30 seconds prior to the cataloged arrival time and the 150 seconds subsequent to the arrival. The only pre-processing applied to the raw data was a normalization, de-trending and bandpass filtering between 0.02 Hz and 10 Hz.

The first four years (2006, 2007, 2008, 2009) are selected as the training set, and the following year (2010) is the validation set. The training and validation sets contained 24,811 and 5,711 seismograms, respectively. To create the training and validation triples, a generator



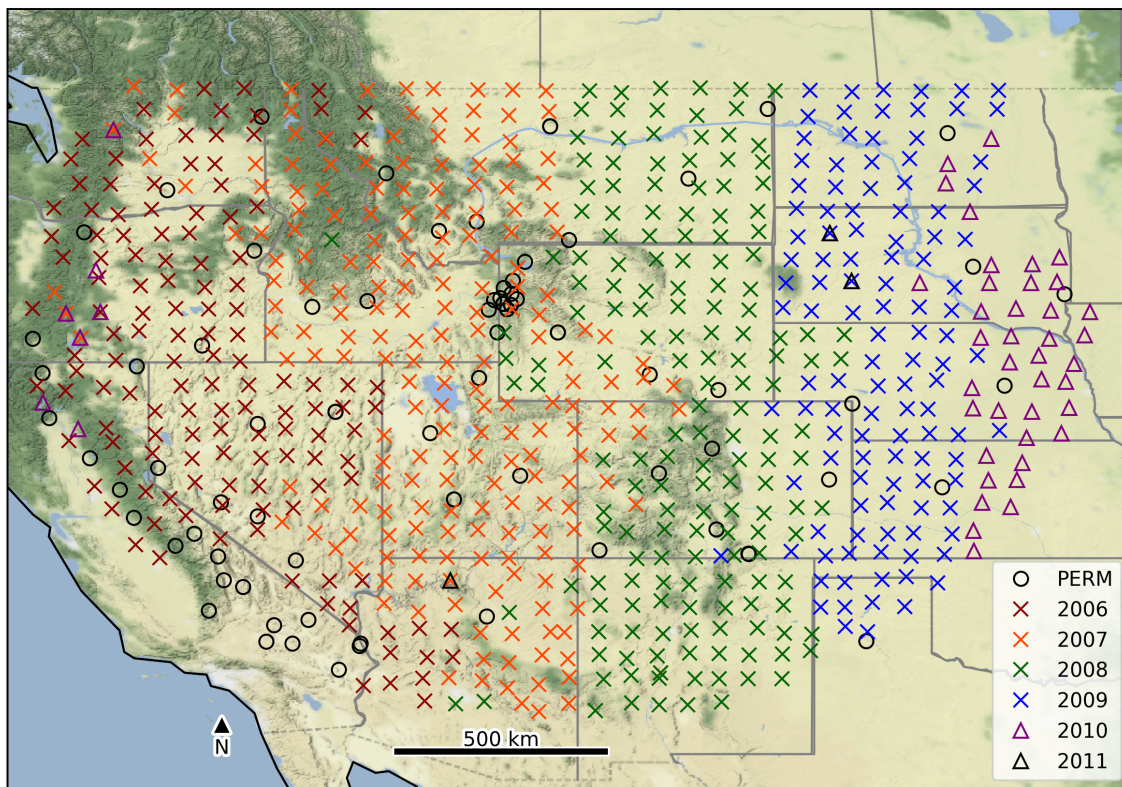


Figure 5: Map showing the geographical location of each recording station in the dataset. The majority of the stations were installed as part of the Transportable USArray, and were in operation from 18 to 24 months before being moved. These stations have been color-coded to show the year of installation. Additionally, stations from the training set are marked with an x, while stations found only in the test and validation sets are marked with a  $\Delta$ . Finally, several permanent stations were also used in this dataset, and have been labeled as ‘PERM’.

function randomly selects an anchor, as well as positive (same event, different station) and negative (different) events. Due to multiple site recordings of many of the individual events (on average, each event was recorded by 30 different stations), there are upwards of 300 million possible triples, which makes this a robust training set for learning seismogram similarity.

The test set was extracted from the last year of the dataset, 2011, and included 4,214 seismogram recordings of 199 unique events taken at 85 stations. All of the events in the test set are mutually exclusive with the training and validation data. Additionally, because of the stations in the array were relocated over time, roughly 10% of these seismograms were recorded by novel stations that were also not present in the same locations in training data. A good performance on these novel data would be evidence of the generalization of the technique.

Three datasets are needed for evaluation of the three tasks: event association, signal detection, and source discrimination. To create the test set for the event association task, 100,000 pairs of seismograms, equally divided into 50,000 matching pairs (where both seismograms captured the same seismic event) and 50,000 non-matching pairs (where the two seismograms captured different seismic events) were assembled. The signal detection task uses a test set containing continuous waveforms for the full five-year dataset across the three stations with the most cataloged arrivals: K22A, K24A, I25A. The test set for the source discrimination task is comprised of a subset of the 4,214 seismograms in the whole test set containing only the primary arrivals - this subset contains 924 seismograms. Positive class labels are applied to all waveforms identified as explosions by the US Geological Survey (640 waveforms) and negative class labels are applied to the remaining 284 waveforms.

## Evaluation Criteria

To demonstrate the performance of the similarity measure, it is applied to three tasks: waveform association, signal detection and source discrimination. Evaluation criteria for each of these tasks is shown below.

Event association is the process of correctly associating the arriving seismic phases of a single event across a network, and is a critical step in seismic analysis. The traditional

algorithms used for this task have always been based on travel times and earth velocity models, however our method is similarity-based: we associate the seismograms entirely based on their similarity in the embedding space, with no external information about arrival times or recording locations. This is a binary classification task: given a pair of seismograms,  $X_A$  and  $X_B$ , the algorithm must classify the pair as matched or unmatched, where a matched pair is defined as two seismogram recordings of the same event. Classification is accomplished by comparing the similarity-based test statistic,  $S$ , against a user defined threshold,  $\tau$ , as seen in Eq. (6).

$$\begin{aligned}
H_0: & \text{ UNMATCHED } (X_A \text{ and } X_B \text{ depict distinct events}) \\
H_A: & \text{ MATCHED } (X_A \text{ and } X_B \text{ depict a common event}) \\
S = & \frac{1}{\left\langle f(X_A), f(X_B) \right\rangle} \\
& \text{reject } H_0 \text{ if } S \geq \tau
\end{aligned} \tag{6}$$

To report performance, a receiver operating characteristic (ROC) curve is built by varying  $\tau$  across the full range of  $S$ , and plotting the rate of false positives against the rate of false negatives for each  $\tau$ . Additionally, for the threshold  $\tau$  which maximizes accuracy, area under the ROC curve (AUC), binary classification accuracy, precision and recall are shown. The evaluation is performed across the 100,000 pairs of seismograms in the waveform association test set, and compared directly against the results found in (Delorey et al., 2019).

Signal detection is defined as a binary classification task, where unlabeled seismogram partitions,  $X$ , are classified as either signal or noise. The determination is based on  $X$ 's embedding space similarity to a set of seismogram templates,  $\{X_1 \dots X_T\}$ , which depict known seismic signals. This is shown in Eq. (7).

$$\begin{aligned}
H_0: & \text{ NOISE } (X \text{ depicts noise}) \\
H_A: & \text{ SIGNAL } (X \text{ depicts signal}) \\
S = & \max_{t=1 \dots T} \frac{1}{\left\langle f(X), f(X_t) \right\rangle} \\
& \text{reject } H_0 \text{ if } S \geq \tau
\end{aligned} \tag{7}$$

The test is performed against a full year of data from two sensors, K22A, I25A. The partitions are 180 seconds long, with a stride of 9 seconds, resulting in an overlap of 95%. Performance of our similarity-based detector is compared to a traditional matched filter technique, which is formulated identically, except the similarity-based test statistic is replaced with cross-correlation, such that  $S = \max_{t=1\dots T} \text{Corr}(X, X_t)$ . ROC curve, AUC, accuracy, precision, and recall are presented.

The source discrimination task is also formulated as binary classification, where unlabeled seismograms  $X$  are classified as either explosion or earthquake, based on their embedding space similarities to both the centroid of a set of explosion templates,  $X_{EXP}$  and the centroid of a set of earthquake templates,  $X_{EQK}$ . This is shown in Eq. (8), where  $\epsilon$  is machine precision.

$$\begin{aligned}
H_0: & \text{ EARTHQUAKE } (X \text{ depicts an earthquake}) \\
H_A: & \text{ EXPLOSION } (X \text{ depicts an explosion}) \\
S = & \frac{\langle f(X), f(X_{EQK}) \rangle}{\langle f(X), f(X_{EXP}) \rangle + \epsilon} \\
& \text{reject } H_0 \text{ if } S \geq \tau
\end{aligned} \tag{8}$$

The test is performed against the full 924 seismograms in the test set. The ROC curve, AUC, accuracy, precision, and recall are presented.

## RESULTS

In this section, we report the performance of our similarity measure across three common tasks in seismology: event association, signal detection and source discrimination. For the signal detection task, we also compare our results to that of a basic correlation detector.

### Waveform Association

To demonstrate that event association using this technique is possible, two sets of measurements are computed in the embedding space: the set of distances between pairs of

seismograms that originate from common events and the set of distances between pairs from different events. As expected the distribution of common-pair distances are lower than the different-pair distances, as shown in Fig. 6.

The ROC curve for the task has an AUC of 85.1% as shown in Fig. 7. The overall accuracy is 79.6% with a precision and recall of 80% and 83%, respectively, and our results are nearly identical to the 80% accuracy reported in (Delorey et al., 2019). Performance is also investigated with respect to the distance between recording stations. As noted previously, correlation-based seismogram similarity is known to decay exponentially with an increase in the distance between recording stations. Our path-invariant measure is also negatively affected by increasing this distance, but the effect is much less pronounced, as demonstrated in Table 2.

Table 2: Waveform Association Performance vs Inter-station Distance

<b>Distance (km)</b>	<b>P</b>	<b>R</b>	<b>Acc</b>
0000-0250	0.833	0.830	0.832
0250-0500	0.804	0.836	0.816
0500-0750	0.754	0.780	0.763
0750-1000	0.757	0.746	0.753
1000-1250	0.735	0.684	0.719

To further investigate the ability of the embedding space to facilitate event association, Fig. 8, displays 100 seismogram embeddings in 2-dimensions using t-Distributed Stochastic Neighbor Embedding (t-SNE). t-SNE minimizes the divergence between two distributions: a distribution that measures pairwise similarities of the input objects and a distribution that measures pairwise similarities of the corresponding low-dimensional points in the embedding (Maaten and Hinton, 2008). The figure clearly demonstrates a clustering of embeddings of common events. However, there are obviously other clusters present as well, shown by the dashed lines in the plot. As it turns out, these other clusters can be incredibly useful, and are explored further in the discussion of the source discrimination task.

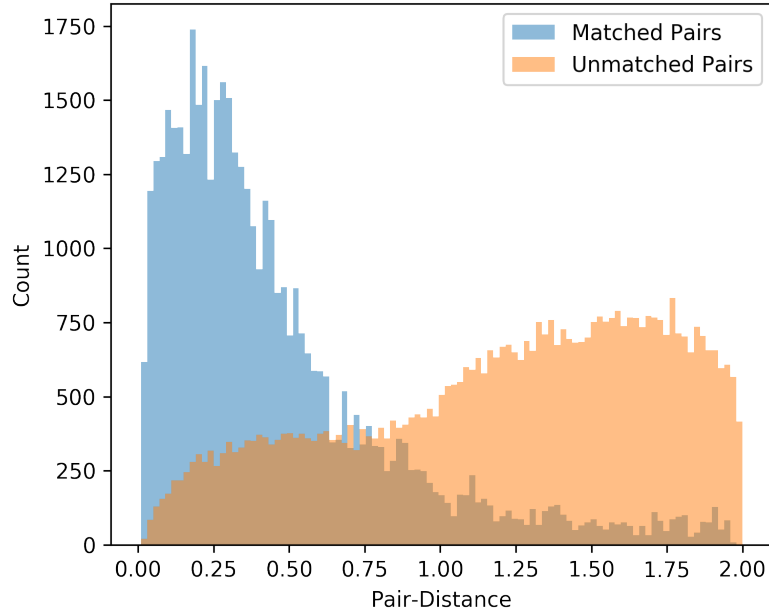


Figure 6: **Blue:** Histogram showing the distribution of embedding space distances between 50,000 pairs of seismograms where each pair are signals from the same event. **Orange:** Histogram showing the distribution of embedding space distances between 50,000 pairs of seismograms where each pair contains different event identifications. The two distributions show that embedding space distances of less than one are much more likely to be associated with matched pairs.

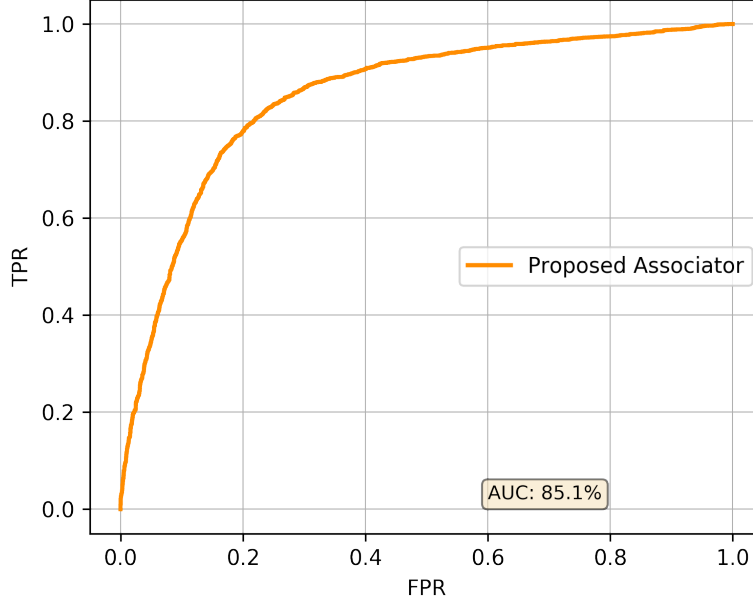


Figure 7: Receiver Operating Characteristic Curve for the Event Association task. The overall area under the curve is 85.1%.

## Signal Detection

We next explore the ability of the similarity measure to facilitate template-based signal detection, reporting performance at K22A, the most active station in the test set. Templates were obtained by extracting 180-second windows for all cataloged arrivals in the training set, such that the window includes 30 seconds prior to arrival and 150 seconds subsequent to the arrival. Detection was accomplished by thresholding the maximum-template similarity of a sliding 180-second window of data at the station under test. This resulted in an AUC of 91.7% and recall of 76% with a type-I error rate of 0.05%. This compares favorably with traditional correlation detection as shown in Fig. 9.

To further investigate the ability of the embedding space to facilitate signal detection, signals arriving at a new station, I25A, are evaluated without retraining - using only the original template embeddings from K22A. This is a situation that correlation detectors are known to struggle with, as the new station represents new paths. The results are as expected, and the path-invariant detector is able to easily surpass the performance of the traditional detector, as shown in Fig. 10. The results are an AUC of 87% and recall of 43.5% which is

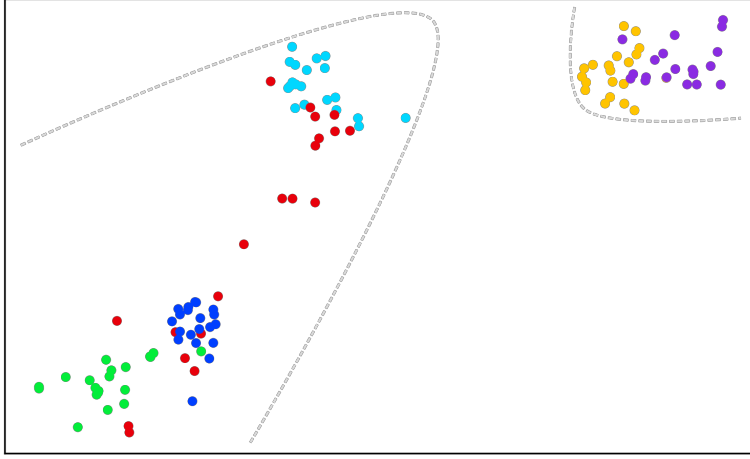


Figure 8: t-SNE Embeddings for Waveform Association. Six unique seismic events were randomly selected from the dataset, along with 20 seismograms for each event, recorded at various stations. These 120 seismograms were then mapped to the 64-dimensional embedding space via the trained neural network. Finally, the 64-dimensional embedding space was visualized here in two dimensions using t-SNE, and each unique event was color-coded. The clustering of same-color embeddings is the result of shared feature commonalities between seismograms of a single event. It is interesting to note that there appears to be some aggregate clustering as well, indicated by the dashed lines. This aggregate clustering is the result of feature commonalities shared across seismograms of multiple events. These inter-event commonalities are explored further, in our results for the source discrimination task.



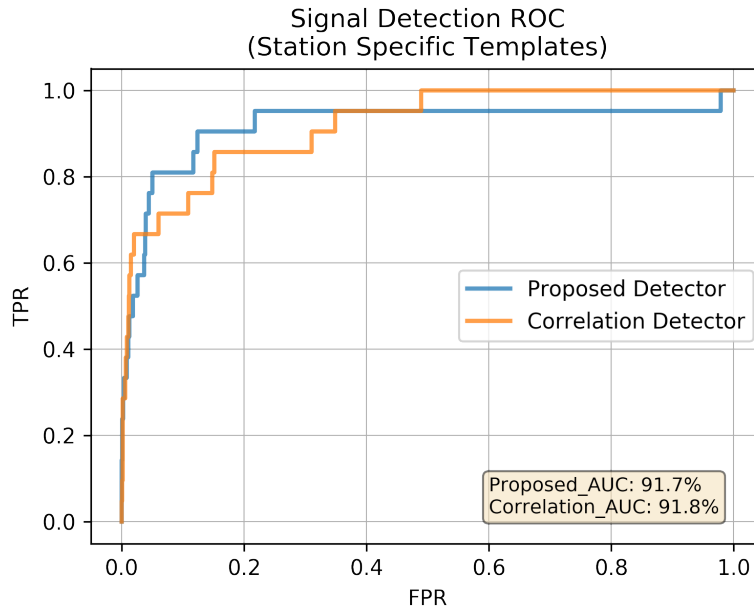


Figure 9: Receiver Operating Characteristic Curve for the signal detection task, with templates taken from the station under test. The orange curve shows the performance of a traditional correlation detector, while the blue curve shows the performance of our proposed embedding space detector.

vastly better than the performance of the correlation detector. The relative locations of the two stations and events are shown in Fig. 11.

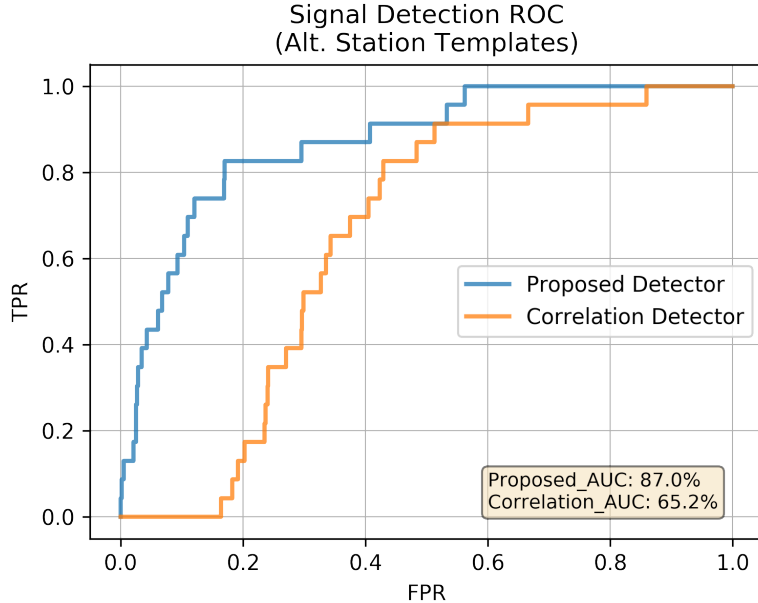


Figure 10: Receiver Operating Characteristic Curve for the signal detection task, with templates taken from a station other than the station under test. The orange curve shows the performance of a traditional correlation detector, while the blue curve shows the performance of our proposed embedding space detector.

## Source Discrimination

Finally, we explore the ability of the similarity measure to facilitate template-based source discrimination. These results are the most impressive, as the network was not explicitly trained in this task. No explicit discrimination labels were used to train the network - the network never had access to any information about whether the training events were earthquakes or explosions. What the network was trained on was source-specificity and path-invariance, which by its very nature should imply a fine-grained extraction of source-specific features and characteristics. It turns out that these features are ideal for source discrimination. The t-SNE visualization of embeddings are labeled with source type (explosion vs earthquake), as shown in Fig. 12. The results show a significant separation between

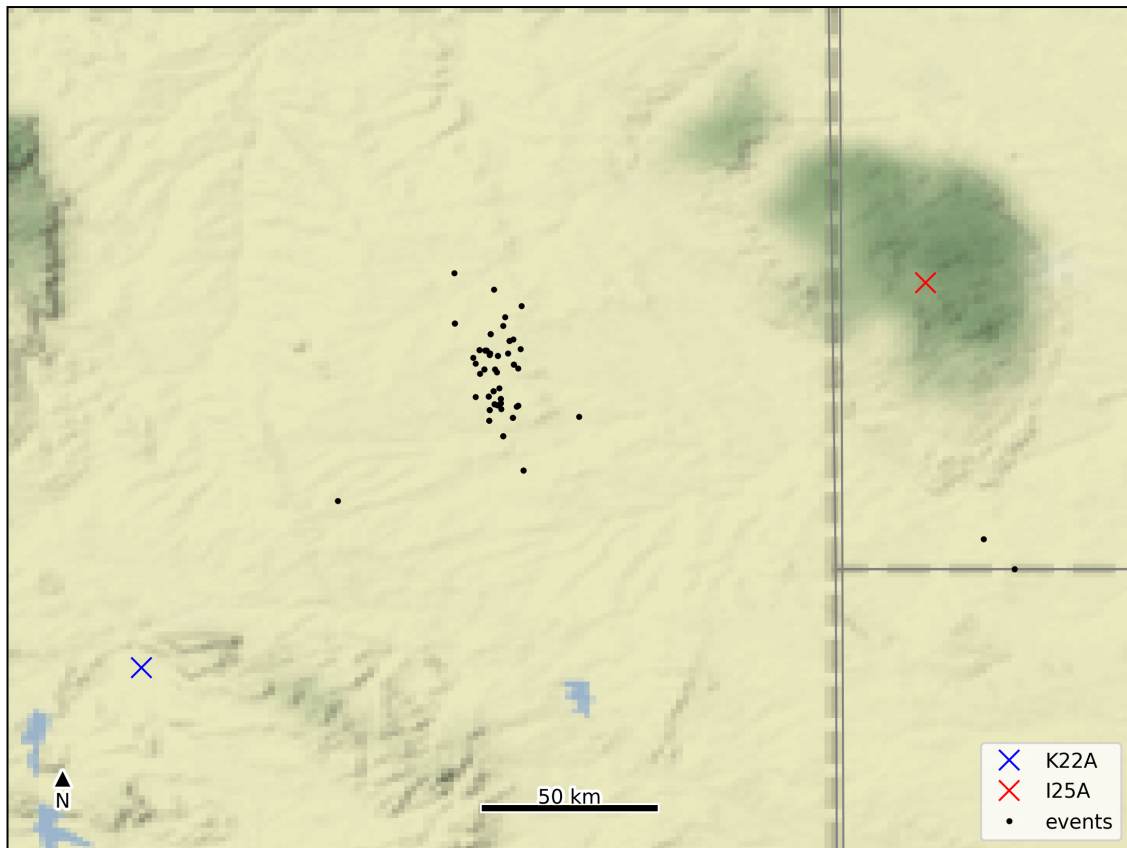


Figure 11: Map showing the locations of both K22A and I25A.

the two source classes in the embedding space, with no other pre-processing or training.

To further evaluate the network on this task, discrimination performance is demonstrated based on different quantities (1, 3, 10 and 100) of randomly-selected exemplar templates. The discriminator achieves a mean AUC of 87.7% for just a single template. This is known as one-shot learning, and enables the creation of a viable classification algorithm with only a single training example. Unfortunately the variance on this AUC is quite high, however, and a few more templates are needed for reliable performance. Fig. 13 shows reliable performance with as few as 10 templates - this method achieves an AUC of 96% with low variance. Choosing the threshold so as to maximize accuracy, the algorithm is then evaluated for accuracy, precision and recall, which are recorded at 90%, 97% and 89% respectively.

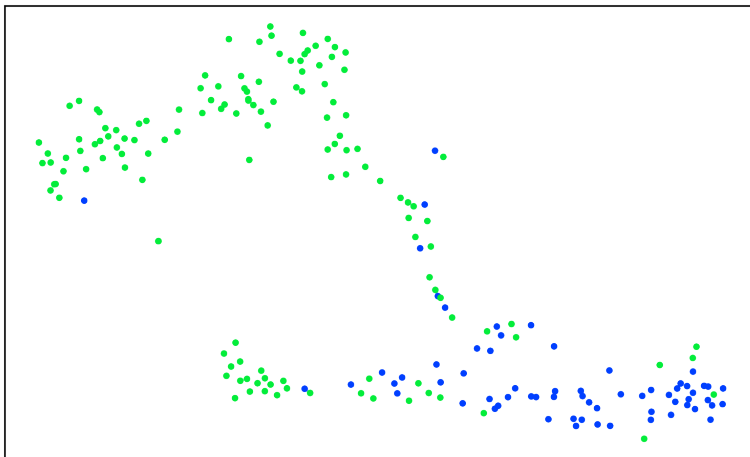


Figure 12: Two-hundred embeddings are shown, visualized in 2D using t-SNE. Blue dots represent explosions and green dots represent earthquakes. The 2D clustering of embeddings demonstrates the inherent association between embeddings with a common source function.

## CONCLUSION

To date, almost all seismogram similarity measures have been based on the cross-correlation function, constraining them to relatively path-dominant similarity, and limiting their use

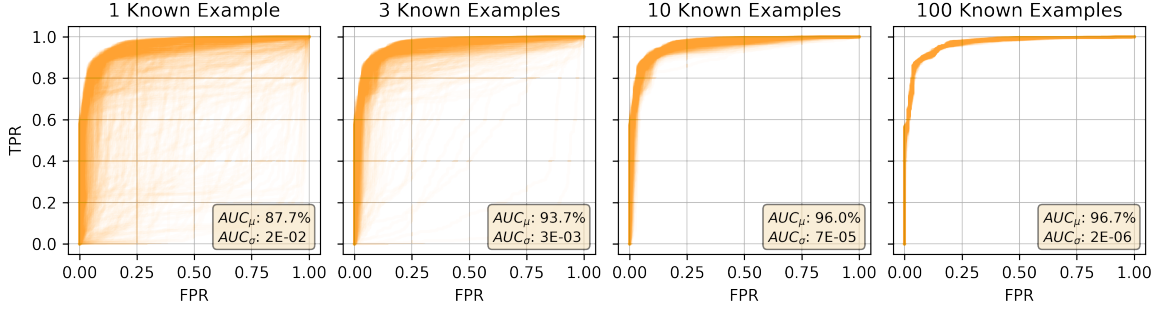


Figure 13: Receiver Operating Characteristic Curves for the Source Discrimination task partitioned to show performance across various numbers of templates. Because the templates are chosen randomly, we have performed 1,000 trials for each figure, plotting the results of each trial as a separate curve. Performance converges nicely for only 10 templates.

to repetitive and geographically localized signals. In this work, we have presented a path-invariant measure for seismogram similarity, based on a deep triplet network architecture, and demonstrated its utility on three common tasks in seismology: event association, signal detection and source discrimination.

For the event association task, the algorithm is able to achieve an accuracy of 80%, without any knowledge of recording time or phase type. These results could be used to augment exiting methods of event association. Future work could focus on constructing a framework for a hybrid technique for event association in an operational setting.

For the signal detection task, there is much work yet to be done. While we have demonstrated the potential of this technique for general signal detection, our algorithm’s performance is compared to that of the most rudimentary correlation detector. Future work should focus on comparing our technique to a state of the art detector, such as that given in (Bergen and Beroza, 2018a). Additionally, we believe that our results here could be augmented by additional training. In particular, our network was trained entirely on seismograms that included active cataloged arrivals, but the general detection task should benefit from retraining the network using a mixture of arrivals and non-arrivals (noise). By supplying the network with a large corpus of noise templates at training time, it is possible that the network would better recognize seismic noise, and increase the overall efficiency of the detector.

Finally, the results for the source discrimination task are quite promising. The 90% classification accuracy achieved for the explosion vs earthquake task is impressive on its own. However it is astounding considering that the discrimination is based on as few as a single template waveform. This result is not only useful for the explosion vs earthquake task, but it also holds considerable promise for future work. For instance, while access to mining explosion templates is extensive, there are other types of anthropogenic events for which we have fewer templates, and it would be interesting to extend these results to such signals. Future work could also focus on clustering in the embedding space, potentially unveiling new classes of signals.

The findings in this work represent an important step forward in the field of seismogram similarity, demonstrating that such similarity measures do not need to be constrained to the path-dominant correlation-based detectors traditionally implemented.

## Data and Resources

The raw seismograms used in this study were collected as part of Earth Scope’s USArray experiment (Busby et al., 2018), and can be accessed via the Incorporated Research Institutions for Seismology (IRIS) Database using ObsPy (Beyreuther et al., 2010).

Arrival-time catalogs for each station were downloaded through a web query of the International Seismological Centre (ISC) Bulletin for seismic arrivals:

<http://www.isc.ac.uk/iscbulletin/search/arrivals/> (last accessed February 2019).

The Neural Network Architecture was implemented in Keras (Chollet and others, 2015), using the keras-tcn python package written by Philippe Rémy:

<https://github.com/philipperemy/keras-tcn> (last accessed February 2019).

The batch-hard algorithm was implemented in Tensorflow (Abadi et al., 2015), and adapted from the work of Olivier Moindrot, which can be found at:

<https://omoindrot.github.io/triplet-loss> (last accessed February 2019).

# Acknowledgment

The results presented in this paper are solely the opinion of the authors; they do not represent the official position or policy of the United States Government.

# References

- Abadi, M., Agarwal, A., Barham, P., Brevdo, E., Chen, Z., Citro, C., Corrado, G. S., Davis, A., Dean, J., Devin, M., Ghemawat, S., Goodfellow, I., Harp, A., Irving, G., Isard, M., Jia, Y., Jozefowicz, R., Kaiser, L., Kudlur, M., Levenberg, J., Mané, D., Monga, R., Moore, S., Murray, D., Olah, C., Schuster, M., Shlens, J., Steiner, B., Sutskever, I., Talwar, K., Tucker, P., Vanhoucke, V., Vasudevan, V., Viégas, F., Vinyals, O., Warden, P., Wattenberg, M., Wicke, M., Yu, Y., and Zheng, X. (2015). {TensorFlow}: Large-Scale Machine Learning on Heterogeneous Systems.
- Bai, S., Kolter, J. Z., and Koltun, V. (2018). An Empirical Evaluation of Generic Convolutional and Recurrent Networks for Sequence Modeling. *CoRR*, abs/1803.0.
- Beaucé, E., Frank, W. B., and Romanenko, A. (2017). Fast Matched Filter (FMF): An Efficient Seismic Matched-Filter Search for Both CPU and GPU Architectures. *Seismological Research Letters*, 89(1):165–172.
- Belkin, M. and Niyogi, P. (2003). Laplacian Eigenmaps for Dimensionality Reduction and Data Representation. *Neural Computation*, 15(6):1373–1396.
- Bergen, K. J. and Beroza, G. C. (2018a). Detecting earthquakes over a seismic network using single-station similarity measures. *Geophysical Journal International*, 213(3):1984–1998.
- Bergen, K. J. and Beroza, G. C. (2018b). Earthquake Fingerprints: Extracting Waveform Features for Similarity-Based Earthquake Detection. *Pure and Applied Geophysics*.
- Beyreuther, M., Barsch, R., Krischer, L., Megies, T., Behr, Y., and Wassermann, J. (2010). ObsPy: A Python Toolbox for Seismology. *Seismological Research Letters*, 81(3):530–533.

- Bormann, P. and IASPEI (2012). *New Manual of Seismological Observatory Practice (NMSOP-2)*, volume 2 Volumes. GFZ German Research Centre for Geosciences, Potsdam, DE, 2 edition.
- Burges, C. J. C., Platt, J. C., and Jana, S. (2003). Distortion discriminant analysis for audio fingerprinting. *IEEE Transactions on Speech and Audio Processing*, 11(3):165–174.
- Busby, R., Woodward, R., Hafner, K., Vernon, F., and Frassetto, A. (2018). The Design and Implementation of EarthScope’s USArray Transportable Array in the Conterminous United States and Southern Canada. Technical report, Earth Scope.
- C. Pechmann, J. and Kanamori, H. (1982). Waveforms and spectra of preshocks and aftershocks of the 1979 Imperial Valley, California, Earthquake: evidence for fault heterogeneity. *Journal of Geophysical Research*, 871:10579–10598.
- Chen, Y., Garcia, E. K., Gupta, M. R., Rahimi, A., and Cazzanti, L. (2009). Similarity-based Classification: Concepts and Algorithms. *J. Mach. Learn. Res.*, 10:747–776.
- Chollet, F. and others (2015). Keras. [\url{https://keras.io}](https://keras.io).
- Chopra, S., Hadsell, R., and LeCun, Y. (2005). Learning a Similarity Metric Discriminatively, with Application to Face Verification. *Proceedings of the IEEE Computer Society Conference on Computer Vision and Pattern Recognition*, 1:539–546.
- Delorey, A. A., McBrearty, I. W., and Johnson, P. A. (2019). Pairwise Association of Seismic Arrivals with Convolutional Neural Networks. *Seismological Research Letters*, 90(2).
- Dickey, J., Borghetti, B., and Juneke, W. (2019). Improving Regional and Teleseismic Detection for Single-Trace Waveforms Using a Deep Temporal Convolutional Neural Network Trained with an Array-Beam Catalog. *Sensors*, 19(3).
- Dodge, D. A. and Walter, W. R. (2015). Initial Global Seismic Cross-Correlation Results: Implications for Empirical Signal Detectors. *Bulletin of the Seismological Society of America*, 105(1):240–256.



- Dysart, P. S. and Pulli, J. J. (1987). Spectral study of regional earthquakes and chemical explosions recorded at the NORESS array. Technical report, Center for Seismic Studies.
- Frankel, A. (1982). Precursors to a magnitude 4.8 earthquake in the Virgin Islands: Spatial clustering of small earthquakes, anomalous focal mechanisms, and earthquake doublets. *Bulletin of the Seismological Society of America*, 72(4):1277–1294.
- Giannakis, G. B. and Tsatsanis, M. K. (1990). Signal detection and classification using matched filtering and higher order statistics. *IEEE Transactions on Acoustics, Speech, and Signal Processing*, 38(7):1284–1296.
- Gibbons, S. J. and Ringdal, F. (2006). The detection of low magnitude seismic events using array-based waveform correlation. *Geophysical Journal International*, 165(1):149–166.
- Hadsell, R., Chopra, S., and LeCun, Y. (2006). Dimensionality reduction by learning an invariant mapping. *Proceedings of the IEEE Computer Society Conference on Computer Vision and Pattern Recognition*, 2:1735–1742.
- Harris, D. B. (1991). A waveform correlation method for identifying quarry explosions. *Bulletin of the Seismological Society of America*, 81(6):2395–2418.
- Harris, D. B. (2006). Subspace Detectors: Theory. Technical report, Lawrence Livermore National Laboratory (LLNL), Livermore, CA.
- Hermans, A., Beyer, L., and Leibe, B. (2017). In Defense of the Triplet Loss for Person Re-Identification. *arXiv e-prints*, abs/1703.0.
- Hoffer, E. and Ailon, N. (2015). Deep metric learning using triplet network. *Lecture Notes in Computer Science (including subseries Lecture Notes in Artificial Intelligence and Lecture Notes in Bioinformatics)*, 9370(1271):84–92.
- Hutchings, L. and Wu, F. (1990). Empirical Green’s Functions from small earthquakes: A waveform study of locally recorded aftershocks of the 1971 San Fernando Earthquake. *Journal of Geophysical Research*, 95:1187–1214.

- Israelsson, H. (1990). Correlation of waveforms from closely spaced regional events. *Bulletin of the Seismological Society of America*, 80(6B):2177–2193.
- Jain, P., Kulis, B., Dhillon, I. S., and Grauman, K. (2008). Online metric learning and fast similarity search. *Advances Neural Information Processing Systems*, pages 1–8.
- Jain, P., Kulis, B., V. Davis, J., and S. Dhillon, I. (2009). Metric and Kernel Learning Using a Linear Transformation. *Journal of Machine Learning Research*, 13.
- Jang, D. and Yoo, C. D. (2009). Fingerprint matching based on distance metric learning. In *2009 IEEE International Conference on Acoustics, Speech and Signal Processing*, pages 1529–1532.
- Kanamori, H. and Ishida, M. (1978). The foreshock activity of the 1971 San Fernando earthquake, California. *Bulletin of the Seismological Society of America*, 68(5):1265–1279.
- Koch, G., Zemel, R., and Salakhutdinov, R. (2015). Siamese neural networks for one-shot image recognition. In *ICML Deep Learning Workshop*, volume 2.
- Kong, Q., Trugman, D. T., Ross, Z. E., Bianco, M. J., Gerstoft, P., and Meade, B. J. (2018). Machine Learning in Seismology: Turning Data into Insights. *Seismological Research Letters*, 90(1):3–14.
- Kumar, V. B. G., Carneiro, G., and Reid, I. (2016). Learning Local Image Descriptors with Deep Siamese and Triplet Convolutional Networks by Minimizing Global Loss Functions. In *IEEE Conference on Computer Vision and Pattern Recognition (CVPR)*, pages 5385–5394.
- Leal-Taixe, L., Canton-Ferrer, C., and Schindler, K. (2016). Learning by Tracking: Siamese CNN for Robust Target Association. *IEEE Computer Society Conference on Computer Vision and Pattern Recognition Workshops*, pages 418–425.
- LeCun, Y., Boser, B., Denker, J. S., Henderson, D., Howard, R. E., Hubbard, W., and Jackel, L. D. (1989). Backpropagation Applied to Handwritten Zip Code Recognition. *Neural Computation*, 1(4):541–551.

- Maaten, L. v. d. and Hinton, G. (2008). Visualizing Data using t-SNE. *Journal of Machine Learning Research*, 9(Nov):2579–2605.
- Motoya, Y. and Abe, K. (1985). Waveform Similarity among Foreshocks and Aftershocks of the October 18, 1981, Eniwa, Hokkaido, Earthquake. In Kisslinger, C. and Rikitake, T., editors, *Practical Approaches to Earthquake Prediction and Warning*, pages 627–636. Springer Netherlands, Dordrecht.
- Schroff, F., Kalenichenko, D., and Philbin, J. (2015). FaceNet: A Unified Embedding for Face Recognition and Clustering. In *CVPR*.
- Schulte-Theis, H. and Joswig, M. (1993). Master-event correlations of weak local earthquakes by dynamic waveform matching. *Geophysical Journal International*, 113(3):562–574.
- Sidiropoulos, P. (2014). N-sphere chord length distribution. *arXiv preprint*.
- Stauder, W. and Ryall, A. (1967). Spatial distribution and source mechanism of microearthquakes in Central Nevada. *Bulletin of the Seismological Society of America*, 57(6):1317–1345.
- Wang, J., Song, Y., Leung, T., Rosenberg, C., Wang, J., Philbin, J., Chen, B., and Wu, Y. (2014). Learning Fine-grained Image Similarity with Deep Ranking. *arXiv e-prints*, page arXiv:1404.4661.
- Xing, E. P., Jordan, M. I., Russell, S., Ng, A. Y., Jordan, M. I., and Russell, S. (2002). Distance metric learning with application to clustering with side-information. *Advances in neural information processing systems (NIPS)*, 15(2):505–512.
- Yoon, C. E., O’Reilly, O., Bergen, K. J., and Beroza, G. C. (2015). Earthquake detection through computationally efficient similarity search. *Science advances*, 1(11):e1501057–e1501057.
- Zhang, M. and Wen, L. (2015). An effective method for small event detection: match and locate (MnL). *Geophysical Journal International*, 200(3):1523–1537.